Supporting Information

Superior Oxygen Electrocatalysts Derived from Predesigned Covalent Organic Polymers for Zinc-Air Flow Batteries

Jianing Guo,[+a] Tingting Li,[+a] Qiuli Wang,[a] Ningyuan Zhang,[a] Yuanhui Cheng,[a] Zhonghua Xiang *[a]

[a] Beijing Advanced Innovation Centre for Soft Matter Science and Engineering, State Key Laboratory of Organic-Inorganic Composites, College of Chemical Engineering, College of Energy, Beijing University of Chemical Technology, Beijing, 100029, PR, China.

[+] Equal contribution

Email: xiangzh@mail.buct.edu.cn

1. Materials

All reagents were obtained from commercial sources and were used without further purification unless otherwise stated. Meso-Tetra (p-bromophenyl) porphine was purchased from Frontier Scientific. 3,8-Dibromophenanthroline was purchased from Changchun Third Party Pharmaceutical Technology Co. Ltd. Nickel(II) chloride was purchased from Energy Chemical. Bis(1,5-cyclooctadiene)nickel(0) ([Ni(cod)$_2$]) and Iron(III)chloride anhydrous was purchased from Strem Chemicals. 1,5-Cyclooctadiene (cod), 2,2'-Dipyridyl, tetraethyl orthosilicate (TEOS) and N,N-dimethylformamide (DMF) were purchased from J&K Chemical Technology. Anhydrous ethanol, trichloromethane, and hydrofluoric acid (HF) were purchased from Beijing Chemical Works. Tetrahydrofuran and formic acid were purchased from Beijing Tong Guang Fine Chemical Company. Commercial Pt/C catalyst, Iridium(IV) oxide (IrO_2) and Carbon black were bought from Alfa Aesar Chemical Co. Ltd. Nafion solution was purchased from DuPont Company.

2. ORR Measurements

The cyclic voltammetry (CV) experiments were conducted in an O_2-saturated 1 M KOH

solution for the ORR from 0.05 to 1.25 V (vs RHE) with a scan rate 100 mV·s^{-1}. RRDE measurements were conducted by liner sweep voltammetry (LSV) from 0.05 to 1.15 V (vs RHE) at a scan rate of 5 mV s^{-1} at 1600 rpm. The number of electrons (*n*) involved in the ORR can be calculated from the Koutecky–Levich (K–L) equation:

$$\frac{1}{J}=\frac{1}{J_L}+\frac{1}{J_K}=\frac{1}{B\omega^{1/2}}+\frac{1}{J_K}$$

$$B=0.62nFC_o(D_o)^{2/3}v^{-1/6}$$

where J is the measured current density, J_K and J_L are the kinetic- and diffusion-limiting current densities, B is the reciprocal of the slope, ω is the angular velocity of the electrode (rad s^{-1}), n is transferred electron number, F is the Faraday constant (F = 96485 C mol^{-1}), Co is the bulk concentration of O_2 (7.8 × 10^{-7} mol cm^{-3}), Do is the O_2 diffusion coefficient (1.43 × 10^{-5} cm^2 s^{-1}), v is the kinematic viscosity of the electrolyte (1 × 10^{-2} cm^2 s^{-1}).

The following equations were used to calculate n (the apparent number of electrons transferred during ORR).

$$n=4\times\frac{I_d}{I_d+I_r/N}$$

where I_d is disk current, I_r is ring current, and N = 0.37 is the current collection efficiency of the Pt ring.

The ORR stability was investigated by continuous potential cycling in O2-saturated 1M KOH solution between 0.65 V and 0.95 V (vs RHE) with the scan rate at 100 mV s^{-1}. And after 5000 cycles, the ORR steady-state polarization measurements were conducted in O2-saturated 1 M KOH solution with scanning rates of 5 mV s^{-1} and rotation rate at 1600 rpm.

3. OER Measurement

OER tests were conducted in an O_2-saturated 1 M KOH electrolyte with a scan rate of 5 mV

s^{-1} at room temperature. The potential range was from 1.05 to 1.85 V (vs RHE). All data were corrected using the iR-correction, where i is the current and R is the electrolyte ohmic resistance, which was obtained via high-frequency A.C impedance. The electrochemical impedance spectroscopy measurements were performed within a frequency range from 1×10^{6} to 1×10^{-3} Hz. Stability was investigated by continuous potential cycling in O_2-saturated 1 M KOH solution between 1.45 V and 1.75 V (vs RHE) with a scan rate of 100 mV s^{-1}. And after 1000 cycles, the OER steady-state polarization measurements were conducted in O2-saturated 1 M KOH solution with scanning rates of 5 mV s^{-1}.

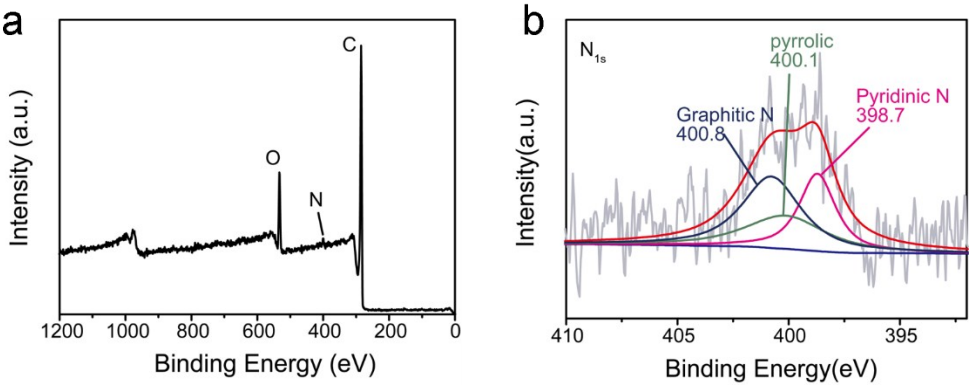

Fig. S1. a) XPS spectra of $CCOP_{TDP}$-FeNi-SiO_2. b) XPS spectra of N 1s for $CCOP_{TDP}$-FeNi-SiO_2.

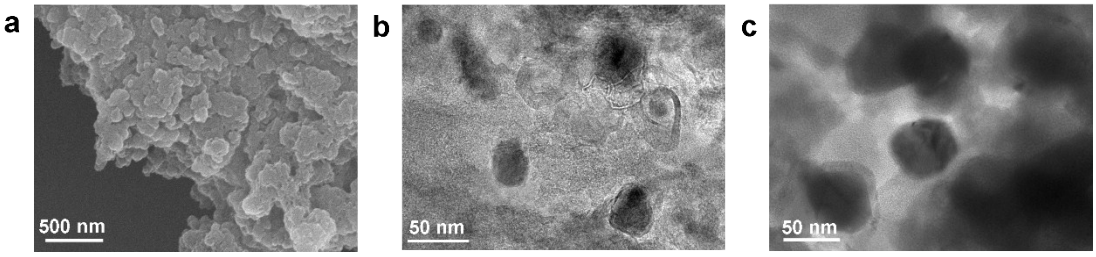

Fig. S2. a) The SEM image for COP_{TDP}. b) HRTEM image of $CCOP_{TDP}$-FeNi-SiO_2. c) HRTEM image of $CCOP_{TDP}$-FeNi.

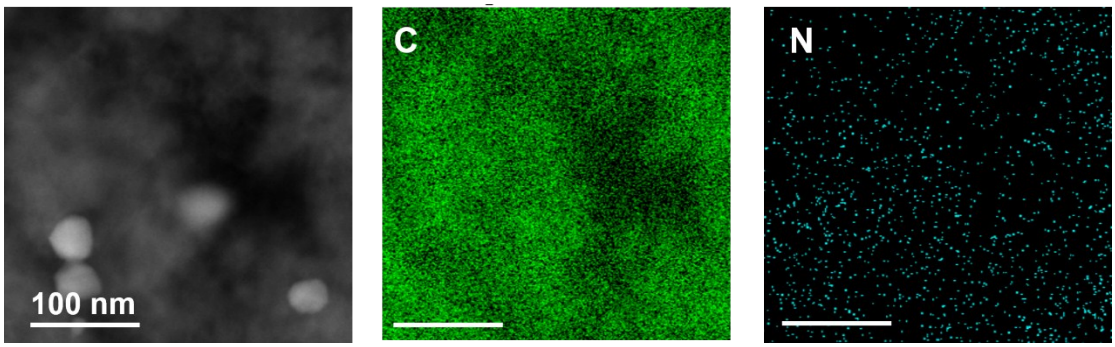

Fig. S3. High-angle annular dark-field (HAADF)-STEM image of $CCOP_{TDP}$-FeNi-SiO_2 and corresponding element maps of C and N elements for $CCOP_{TDP}$-FeNi-SiO_2.

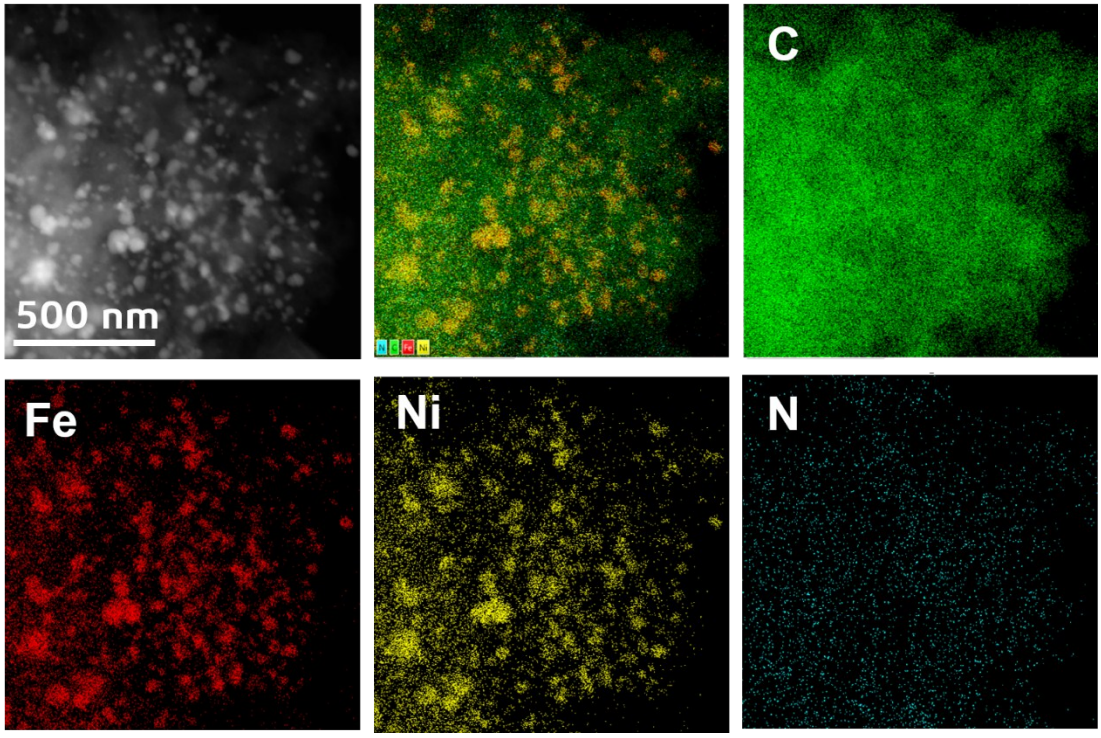

Fig. S4. High-angle annular dark-field (HAADF)-STEM image of $CCOP_{TDP}$-FeNi and corresponding element maps of C, Fe, Ni and N elements for $CCOP_{TDP}$-FeNi.

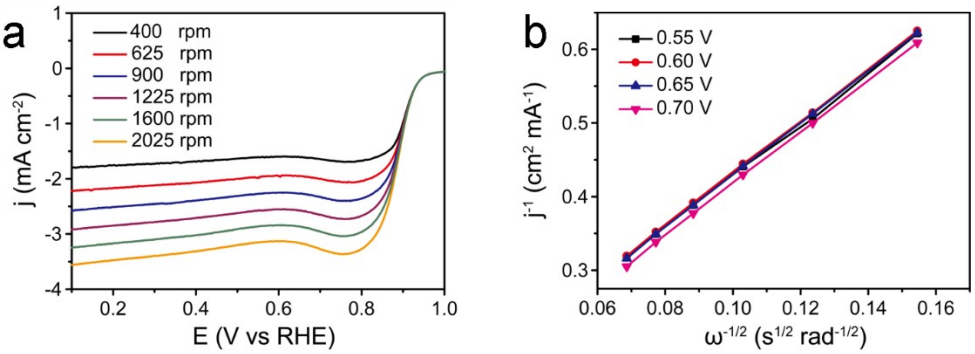

Fig. S5. a) Rotating disk electrode (RDE) linear sweep voltammograms of $CCOP_{TDP}$-FeNi-SiO_2 at different rotating rates in the alkaline solution. b) Koutecky-Levich plots of $CCOP_{TDP}$-FeNi-SiO_2 derived from RDE voltammograms.

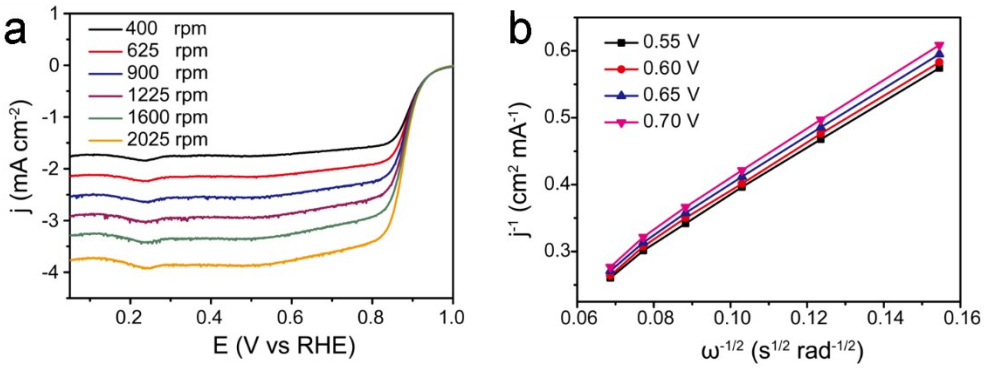

Fig. S6. a) Rotating disk electrode (RDE) linear sweep voltammograms of Pt/C at different rotating rates in the alkaline solution. b) Koutecky-Levich plots of Pt/C derived from RDE voltammograms.

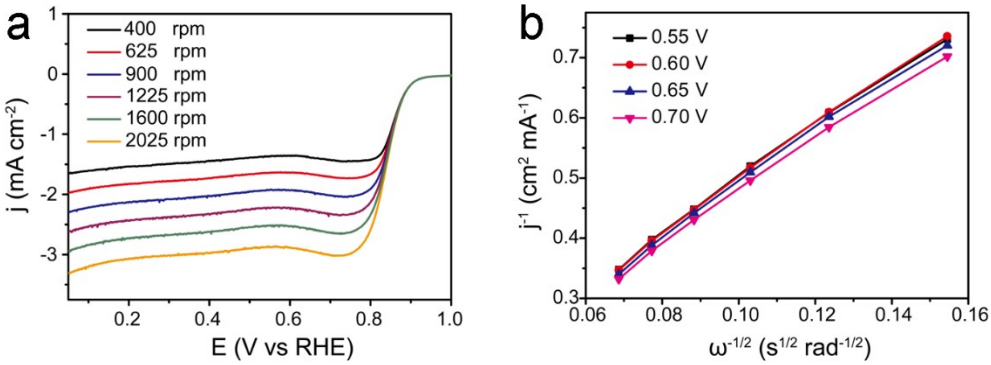

Fig. S7. a) Rotating disk electrode (RDE) linear sweep voltammograms of $CCOP_{TDP}$-FeNi at different rotating rates in the alkaline solution. b) Koutecky-Levich plots of $CCOP_{TDP}$-FeNi derived from RDE voltammograms.

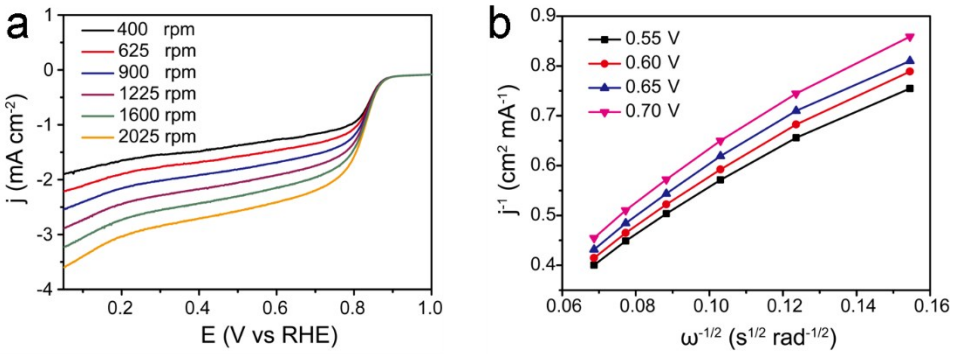

Fig. S8. a) Rotating disk electrode (RDE) linear sweep voltammograms of $CCOP_{TDP}$ at different rotating rates in the alkaline solution. b) Koutecky-Levich plots of $CCOP_{TDP}$ derived from RDE voltammograms.

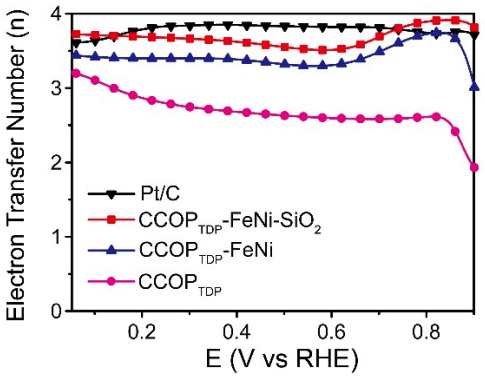

Fig. S9. Electron transfer number.

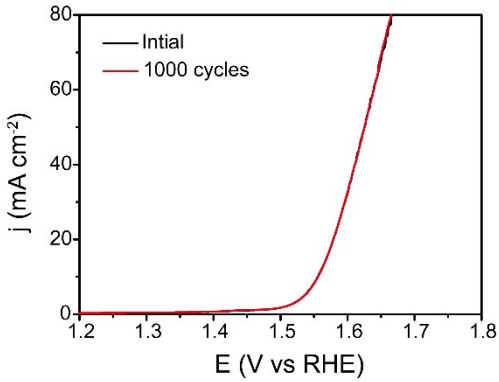

Fig. S10. OER LSV curves of CCOP$_{TDP}$-FeNi-SiO$_2$ before and after 1 000 potential cycles ranging from 1.45 V and 1.75 V (vs RHE) in O_2-saturated 1 M KOH.

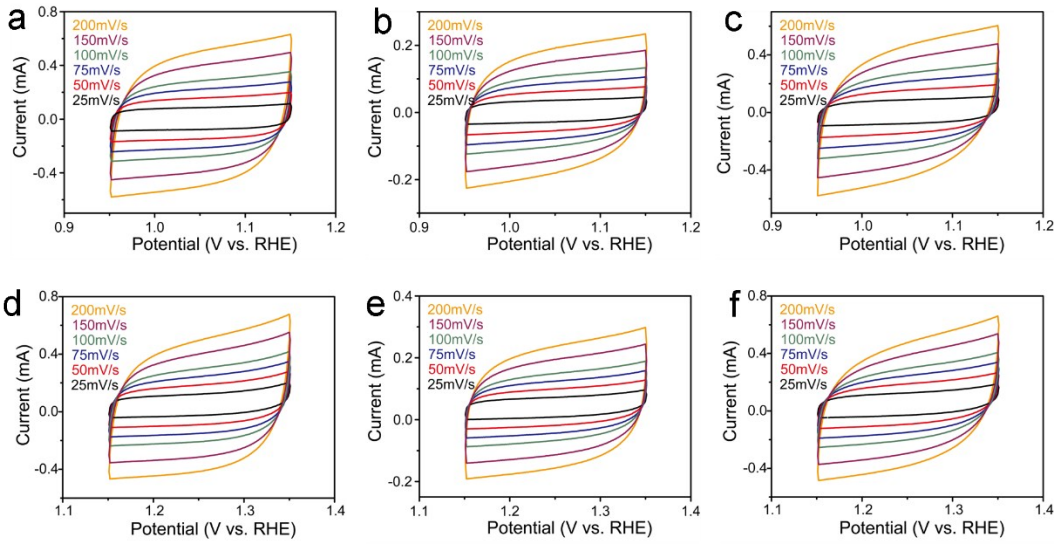

Fig. S11. a), b) and c) Cyclic voltammograms at various scan rates between 0.95 and 1.15 V vs. RHE for ORR in nitrogen saturated 1M KOH electrolyte for $CCOP_{TDP}$-FeNi-SiO_2, $CCOP_{TDP}$-FeNi and $CCOP_{TDP}$, respectively. d), e) and f) Cyclic voltammograms at various scan rates between 1.15 and 1.35 V vs. RHE for OER in nitrogen saturated 1M KOH electrolyte for $CCOP_{TDP}$-FeNi-SiO_2, $CCOP_{TDP}$-FeNi and $CCOP_{TDP}$, respectively.

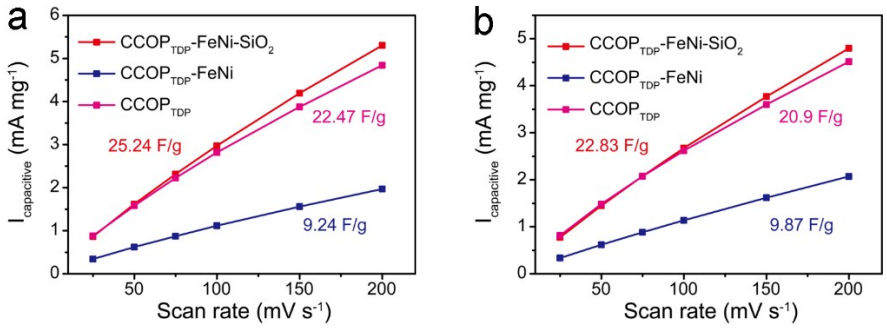

Fig. S12. a) The capacitive current at 1.05 V vs RHE for ORR at various scan rates for $CCOP_{TDP}$-FeNi-SiO_2, $CCOP_{TDP}$-FeNi and $CCOP_{TDP}$, respectively. b) The capacitive current at 1.25 V vs RHE for OER at various scan rates for $CCOP_{TDP}$-FeNi-SiO_2, $CCOP_{TDP}$-FeNi and $CCOP_{TDP}$, respectively.

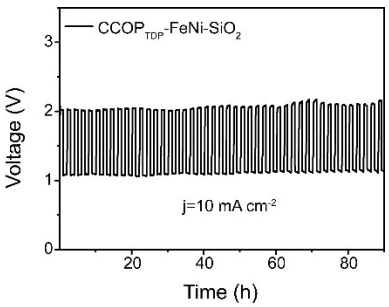

Fig. S13. Charge-discharge cycling performance of a rechargeable Zn-air flow battery based on $CCOP_{TDP}$-FeNi-SiO_2 electrocatalyst at a current density of 10 mA cm^{-2}.

Table S1. The comparison of the catalytic activity toward the ORR and OER in 1 M KOH or 1 M NaOH of the $CCOP_{TDP}$-FeNi-SiO_2 with other reported catalysts.

Catalyst	Loading ug/cm^2	Electrolyte	$E_{ORR,\ overpotential}$	$E_{1/2}$/ V	$E_{OER,\ overpotential\ @10mA\ cm^{-2}}$/V	ΔE/ V	Ref
$FeNi_2Se_4$–NrGO	450	1M KOH	0.3	~0.6	0.17	0.8	[1]
N-GT(FeCoNi)	600	1M NaOH	0.22	0.89	~0.32	0.66	[2]
NCNT/CoONiO-NiCo	210	1M KOH	0.26	0.83	0.27	0.67	[3]
N-CG–CoO	220	1M KOH	~0.33	0.81	0.34	0.76	[4]
NC-Co_3O_4-90	/	1M KOH	0.32	0.87	0.36	0.72	[5]
$(\alpha\text{-}MnO_2)_2$-$(LaNiO_3)_3$/CNTs	500	1M KOH	~0.4	0.69	0.55	1.09	[6]
$MnNiCoO_4$/N-MWCNT	260	1M KOH	0.28	0.88	0.39	0.74	[7]
Co_4N/CNW/CC	/	1M KOH	~0.33	0.80	0.31	0.74	[8]
Co_3O_4@N-rmGO	100	1M KOH	~0.27	~0.88	0.31	0.74	[9]
NCNT/$CoxMn_{1-x}O$	210	1M KOH	0.27	0.84	0.34	0.73	[10]
$CCOP_{TDP}$-FeNi-SiO_2	386	**1M KOH**	**0.24**	**0.89**	**0.31**	**0.65**	**This work**

$\Delta E = E_{j=10,\ OER} - E_{1/2,\ ORR}$

$E_{ORR,\ overpotential} = 1.23 - E_{onset\ potential}$

$E_{OER,\ overpotential@10mA\ cm^{-2}} = E_{j=10mA\ cm^{-2}} - 1.23$

Table S2. The element analysis of $CCOP_{TDP}$-FeNi and $CCOP_{TDP}$-FeNi-SiO_2

Sample	C(%)	N(%)
$CCOP_{TDP}$-FeNi	66.66	3.28
$CCOP_{TDP}$-FeNi-SiO_2	88.42	1.39

Table S3. The ICP test of $CCOP_{TDP}$-FeNi and $CCOP_{TDP}$-FeNi-SiO_2

Sample	Fe (%)	Ni (%)
$CCOP_{TDP}$-FeNi	6.20	9.13
$CCOP_{TDP}$-FeNi-SiO_2	0.72	0.91

Reference

[1] S. Umapathi, J. Masud, A. T. Swesi, M. Nath, *Adv. Sustainable Systems* **2017**, *1*, 1700086.

[2] S. Gupta, L. Qiao, S. Zhao, H. Xu, Y. Lin, S. V. Devaguptapu, X. Wang, M. T. Swihart, G. Wu, *Adv. Energy Mater.* **2016**, *6*, 1601198.

[3] M. P. Xien Liu, Min Gyu Kim, Shiva Gupta, Gang Wu, Jaephil Cho, *Angew. Chem. Int. Ed.* **2015**, *54*, 9654.

[4] S. Mao, Z. Wen, T. Huang, Y. Hou, J. Chen, *Energy Environ. Sci.* **2014**, *7*, 609.

[5] C. Guan, A. Sumboja, H. Wu, W. Ren, X. Liu, H. Zhang, Z. Liu, C. Cheng, S. J. Pennycook, J. Wang, *Adv. Mater.* **2017**, *29*.

[6] H. Ma, B. Wang, *RSC Adv.* **2014**, *4*, 46084.

[7] X. Yu, A. Manthiram, *Catal. Sci. Technol.* **2015**, *5*, 2072.

[8] F. Meng, H. Zhong, D. Bao, J. Yan, X. Zhang, *J. Am. Chem. Soc.* **2016**, *138*, 10226.

[9] Y. Liang, Y. Li, H. Wang, J. Zhou, J. Wang, T. Regier, H. Dai, *Nat. Mater.* **2011**, *10*, 780.

[10] X. Liu, M. Park, M. G. Kim, S. Gupta, X. Wang, G. Wu, J. Cho, *Nano Energy* **2016**, *20*, 315.